DRAFT VERSION JANUARY 30, 2020
Typeset using LaTeX **twocolumn** style in AASTeX62

arXiv:2001.08713v2 [astro-ph.CO] 29 Jan 2020

H_0 Reconstruction with Type Ia Supernovae, Baryon Acoustic Oscillation and Gravitational Lensing Time-Delay

Meng-Zhen Lyu[1], Balakrishna S. Haridasu[2,3], Matteo Viel[4,5,6,7], and Jun-Qing Xia[1]

[1]*Department of Astronomy, Beijing Normal University, Beijing 100875, China*
[2]*Dipartimento di Fisica, Università di Roma "Tor Vergata", Via della Ricerca Scientifica 1, I-00133, Roma, Italy*
[3]*Sezione INFN, Università di Roma "Tor Vergata", Via della Ricerca Scientifica 1, I-00133, Roma, Italy*
[4]*SISSA-International School for Advanced Studies, Via Bonomea 265, 34136 Trieste, Italy*
[5]*INFN, Sezione di Trieste, Via Valerio 2, I-34127 Trieste, Italy*
[6]*INAF - Osservatorio Astronomico di Trieste, Via G. B. Tiepolo 11, I-34143 Trieste, Italy*
[7]*IFPU, Institute for Fundamental Physics of the Universe, via Beirut 2, 34151 Trieste, Italy*

Abstract

There is a persistent H_0-tension, now at more than $\gtrsim 4\sigma$ level, between the local distance ladder value and the *Planck* cosmic microwave background measurement, in the context of flat ΛCDM model. We reconstruct $H(z)$ in a cosmological-model-independent way using three low-redshift distance probes including the latest data from baryon acoustic oscillation, Type Ia supernova and four gravitational lensing Time-Delay observations. We adopt general parametric models of $H(z)$ and assume a Gaussian prior on the sound horizon at drag epoch, $r_{\rm s}$, from *Planck* measurement. The reconstructed H_0 using Pantheon SN Ia and BAO data are consistent with the *Planck* flat ΛCDM value. When including the GLTD data, H_0 increases mildly, yet remaining discrepant with the local measurement at $\sim 2.5\sigma$ level. Our reconstructions being blind to the dark sectors at low redshift, we reaffirm the earlier claims that the Hubble tension is not likely to be solved by modifying the energy budget of the low-redshift universe. We further forecast the constraining ability of future realistic mock BAO data from DESI and GLTD data from LSST, combining which, we anticipate that the uncertainty of the inferred H_0 would be improved by $\sim 38\%$, reaching $\sigma_{H_0} \approx 0.56$ uncertainty level.

Key words: cosmology: observations, distance scale - gravitational lensing: strong - supernovae

1. Introduction

The flat ΛCDM model is a remarkably successful cosmological model. It describes well many observational results, especially at large scales, including the cosmic microwave background (CMB) radiation, light element abundance as the relic of Big Bang nucleosynthesis, galaxy clustering, Lyman-α forest observations and also low redshift distance probes. However, there exists a strong tension for the present Hubble expansion rate (H_0), between the direct measurement using distance ladder of local Universe (Riess et al. 2016, 2019; Yuan et al. 2019), and the *Planck* estimate (Ade et al. 2016; Aghanim et al. 2018) from CMB within the context of ΛCDM (Bernal et al. 2016; Verde et al. 2019; Raveri & Hu 2019). One important aspect is that the discordance, since the first release of *Planck* data (Ade et al. 2014), has become even more prominent due to the improved precision of both these measurements which are at $\sim 9\%$ difference, now reaching a significance of $\gtrsim 4\sigma$ (Riess et al. 2019). More recent low-redshift gravitational lensing time-delay measurements, independent of the local distance ladder, also a the tension at high significance Wong et al. (2019). The H_0 tension, persisting and severely increasing, indicates that it should not merely be regarded as a statistical fluctuation, and is more likely to point to a failure of the standard ΛCDM model, as also noted in Verde et al. (2019), or due to unknown systematics in the data.

CMB provides a stringent constraint on H_0 by combining the measurements of angular location and relative height of the acoustic oscillation of the baryon-photon fluid frozen at last scattering surface at $z \approx 1100$. However, the measurement is model-dependent and influenced by possible extensions to the ΛCDM model, such as the dark energy equation of state parameter w[1] or the curvature $\Omega_{\rm k}$, which as is well-

Corresponding author: Meng-Zhen Lyu
lvmz@mail.bnu.edu.cn
haridasu@roma2.infn.it
viel@sissa.it
xiajq@bnu.edu.cn

[1] One possible way to relieve the Hubble tension is allowing phantom dark energy (Vagnozzi 2019; Di Valentino et al. 2017a). This might however have discrepancy with the low redshift BAO measurements, which con-

known further aggravates the tension. Thus modifying either the early or the local Universe physics can, in principle, alter the H_0 constraints from CMB measurements.

Modification to the ΛCDM model often involves ingredients beyond the standard physics, although the existence of dark matter and dark energy within the ΛCDM framework has already established the necessity for "new" physics. Preferable approaches can be to modified dark energy model and different gravitational field behavior (Di Valentino et al. 2018b; Huang & Wang 2016; Di Valentino et al. 2017a; Zhao et al. 2017; Poulin et al. 2018; Choi et al. 2019; Banihashemi et al. 2019; Khosravi et al. 2019; Umiltà et al. 2015; Rossi et al. 2019; Ballardini et al. 2016), such as an early dark energy (Xia & Viel 2009; Karwal & Kamionkowski 2016; Poulin et al. 2019; Mortsell & Dhawan 2018; Ye & Piao 2020), interaction between dark sectors (Ko & Tang 2016; Raveri et al. 2017; Di Valentino et al. 2018a; Archidiacono et al. 2019), interacting dark energy model (Di Valentino et al. 2017b; Yang et al. 2018; Xia et al. 2013; Pan et al. 2019; Kumar & Nunes 2016) and a family of unified dark matter models (e.g., Camera et al. (2019) and references therein). Apart from the cosmological models, local gravitational potential (Marra et al. 2013), specifically a local void (Keenan et al. 2013; Whitbourn & Shanks 2014) can also partially relieve H_0 tension (Hoscheit & Barger 2017; Shanks et al. 2019), yet there are studies utilizing SN data sets (Kenworthy et al. 2019; Luković et al. 2019), which show that the local structure does not significantly impact measurement of H_0.

Before we turn to revamp the standard ΛCDM model, it is necessary to get some insight from low redshift cosmological probes, whose variousness and observational accuracy can also provide us an integrated and precise understanding of the late universe. In this work, we perform a cosmological-model-independent reconstruction of $H(z)$, an inverse distance ladder analysis using the Type Ia Supernovae (SN Ia), Baryon Acoustic Oscillations (BAO), and Gravitational Lens Time Delays (GLTD) data, which are able to impose a strong constraint on the shape of $H(z)$ and H_0 is simply obtained via extrapolation of $H(z)$ to present ($z = 0$).

GLTD provides a measurement of a combination of distances, when the lens mass model is assumed, the angular diameter distance to the lens can further be obtained. We include the GLTD data as it is an independent distance probe and is an excellent supplement to BAO and SN Ia, even though its current uncertainties are not comparable to the latter, it has the advantage of measuring the absolute distances, unlike, the SNIa, which need marginalization of the nuisance parameter, i.e, standardized absolute luminosity.

Our analyses are closely related to the recent work by (Lemos et al. 2019) (hereafter L18), as we adopt the same parametric form of $H(z)$ and update the BAO data, include the GLTD data into analyses. We find that the reconstructed $H(z)$ nearly reproduces the one of the ΛCDM model. Our inferred H_0 when combining all three probes is slightly higher than the primary results of L18, which is mostly due to the inclusion of GLTD data, which predicts a higher H_0 than the *Planck* ΛCDM estimate. Compared to L18 we also include different priors on the parameters and different Bayesian statistical indicators to assess which models are preferred and the degree of degeneracy of the parameters. As a more important extension, we forecast the performance of future BAO data from the Dark Energy Spectroscopic Instrument (DESI) (Levi et al. 2013) and GLTD data from the Large Synoptic Survey Telescope (LSST) (Ivezic et al. 2019). The forthcoming data from these two future surveys are expected to provide a much tighter constraint on the reconstructed H_0.

The paper is organized as follows: In Section 2 we introduce the parameterization methods of $H(z)$. In Section 3, we present the data used to reconstruction as well as the inference method. We show the final results using the current and future data in Section 4 and then follow the discussion and summary in Section 5.

2. Model and Equations

Firstly, we parameterize $H(z)$ in the following two ways:

$$\left(\frac{H(z)}{H_{0,\mathrm{fid}}}\right)^2 = A_1(1+z)^3 + B_1 + C_1 z + D_1(1+z)^{\epsilon}, \quad (1)$$

$$\left(\frac{H(z)}{H_{0,\mathrm{fid}}}\right)^2 = A_2(1+z)^3 + B_2 + C_2 z + D_2 \ln(1+z), \quad (2)$$

which are the same as in L18, and denote them as Epsilon model and Log model, respectively. While these models serve the purpose of being blind to the dark energy equation of state, they are clearly inadequate to account for the curvature freedom. Moreover, ignoring the curvature would induce error that grows rapidly with redshift in reconstructing the dark energy equation of state (Clarkson et al. 2007). To accommodate for this we also implement two additional models:

$$\left(\frac{H(z)}{H_{0,\mathrm{fid}}}\right)^2 = A_3(1+z)^3 + B_3(1+z)^2 + C_3 + D_3 \ln(1+z), \quad (3)$$

$$\left(\frac{H(z)}{H_0}\right)^2 = A_4(1+z)^3 + B_4(1+z)^2 + D_4. \quad (4)$$

They are denoted as Log2 model and Ω_{k}ΛCDM model, respectively. We substitute the term $\propto z$ with a $\propto (1+z)^2$ term for theoretical and practical reasons: $i)$ the latter has cosmological implication for the curvature of the universe, $ii)$ as shown in right panel of Figure 1, the parameters C_2 and D_2 are strongly correlated, which is primarily due to $\ln(1+z) \approx z$ at small redshifts. We also implement the Ω_{k}ΛCDM model, which we write in a similar parametric form as the other models yet implementing restrictions on its parameters: $i)$ H_0 is a free parameter, which is a different

straints better the $w \lesssim -1$ range, see e.g., Bernal et al. (2016); Aubourg et al. (2015); Haridasu et al. (2018b); Park & Ratra (2019).

implementation from other models where $H_{0,\rm rec}$ is a derived quantity, $ii)$ $A_4 + B_4 + D_4 = 1$, which is in fact the consistency relation when rewritten in terms of standard density parameters ($\Omega_{\rm m}+\Omega_{\rm k}+\Omega_\Lambda = 1$). We adopt a fiducial Hubble constant value of $H_{0,\rm fid} = 67.0\,{\rm km\,s^{-1}/Mpc}$. The reconstructed H_0, denoted as $H_{0,\rm rec}$, for each model is deduced at $z = 0$ after extrapolation. The choice of $H_{0,\rm fid}$ does not alter $H_{0,\rm rec}$[2].

In both Log2 and $\Omega_{\rm k}\Lambda$CDM model, having the explicit $(1+z)^2$ term, which has the interpretation of cosmic curvature, the transverse comoving distance $D_{\rm M}$ becomes

$$D_{\rm M}(z) = \begin{cases} \frac{D_H}{\sqrt{\Omega_{\rm k}}}\sinh\left(\frac{\sqrt{\Omega_{\rm k}}D_C(z)}{D_H}\right), & \Omega_{\rm k} > 0 \\ D_C(z), & \Omega_{\rm k} = 0, \\ \frac{D_H}{\sqrt{-\Omega_{\rm k}}}\sin\left(\frac{\sqrt{-\Omega_{\rm k}}D_C(z)}{D_H}\right), & \Omega_{\rm k} < 0 \end{cases} \quad (5)$$

where the comoving distance $D_{\rm C} = c\int_0^z \frac{dz'}{H(z')}$ and $D_H = c/H_0$, c is the speed of light. Thus, the luminosity distance $D_{\rm l}$ and angular diameter distance $D_{\rm A}$ are

$$D_L(z) = D_{\rm M}(z)(1+z),\ D_{\rm A}(z) = D_{\rm M}(z)/(1+z). \quad (6)$$

BAO measurements often involve an effective volume averaged distance, denoted as D_V, and defined as:

$$D_V(z) = \left[D_{\rm M}^2(z)\frac{cz}{H(z)}\right]. \quad (7)$$

Based on Equation (5), the comoving sound horizon $r_{\rm s}(z)$ at drag epoch is obtained by substituting the light speed c with the sound velocity c_s and changing the limit of integral from the early times ($z \to \infty$) to the drag epoch, z_s, which then reads:

$$r_{\rm s}(z_s) = c_s\int_{z_s}^{\infty}\frac{dz'}{H(z')}, \quad (8)$$

where c_s is a function of the ratio of baryon to photon energy density ($\rho_{\rm b}/\rho_\gamma$), $c_s = 1/\sqrt{3(1+3\rho_b/(4\rho_\gamma))}$. Our purpose here is to reconstruct $H(z)$ in a model-independent way, having minimum involvement with the physics of the early universe. Therefore, here we use a $r_{\rm s}$ prior from the *Planck* (Ade et al. 2016), which implies we assume the universe before z_s is the same as depicted by the ΛCDM model. Also, it has been shown that the dark energy and curvature degree of freedom do not modify the expectation of $r_{\rm s}(z_s)$ (Verde et al. 2017; Verde et al. 2017). The $H(z)$ parameterizations in Equations (1) to (3) are valid only in the late universe.

In a strong lens system, light from a background object is bent, maybe by an intervening mass (lens), and multiple images are generated. The lens systems usually show complicate morphologies and this implies that the light rays go through different optical paths in the gravitational potential. In turn, this can be measured if the source has a variation in flux by relying on the difference in the arrival time, i.e., the time delay, of images. By measuring which, we finally obtain a combination of distance information of the lens system denoted as $D_{\Delta\rm t}$ (Narayan 1991; Treu & Marshall 2016)

$$D_{\Delta\rm t} = (1+z_{\rm l})\frac{D_{\rm l}D_{\rm s}}{D_{\rm ls}}, \quad (9)$$

where $z_{\rm l}$ is the redshift of the lens, $D_{\rm l}$ and $D_{\rm s}$ are the angular diameter distance from us to the lens and source, respectively. $D_{\Delta\rm t}$ has the dimension of distance and consequently is inversely proportioned to H_0. Moreover, with a proper assumption of lens mass density profile, one can extract $D_{\rm l}$ by combining it with the lens stellar velocity dispersion measurements and time-delay measurements (Paraficz & Hjorth 2009; Jee et al. 2015).

3. Data sets and Inference Method

Our work is mainly based on the following three probes: SN Ia, BAO, and GLTD. In this section, we summarize in detail the data used in the reconstruction of $H(z)$. Following which the inference method is also presented.

3.1. *Data sets*

- SNIa from the new Pantheon sample (Scolnic et al. 2018), contains a total of 1048 SN Ia spanning the redshift range from $0.01 < z < 2.3$. The Pantheon sample is a large combination of SN Ia from various surveys, including a subset of 279 SN Ia from the Pan-STARRS1 (PS1) Medium Deep Survey, SDSS, SNLS, various low-z, and HST samples. It has been widely used to constrain cosmology model and in particular, the nature of dark energy. For a given dark energy model, the Pantheon SNIa give consistent constraints on dark energy parameters with the results obtained using the joint light-curve analysis SNIa (Betoule et al. 2014) and also the latest Dark Energy Survey Supernova Program SNIa sample (Abbott et al. 2019).

- Table 1 summarizes the latest BAO measurements used in our reconstruction. We use BAO measurements from 6dF Galaxy Survey (6dFGS) (Beutler et al. 2011) and BOSS DR12 in three redshift bands (Alam et al. 2017). The eBOSS DR14 also provides three high-redshift BAO measurements from quasar (Zarrouk et al. 2018), Lyman-α (Lyα) absorption in the quasar spectrum (Blomqvist et al. 2019), and Lyα-quasar cross-correlation (de Sainte Agathe et al. 2019). In addition, we as well use measurements on $D_{\rm A}(z_{\rm eff})/r_{\rm s}$ and $H(z_{\rm eff})r_{\rm s}$ from eBOSS DR14 luminosity red giants (LRG) analyses at $z_{\rm eff} = 0.72$ (Icaza-Lizaola et al. 2019). We assume two measurements from eBOSS DR14 LRG are independent, as their covariance is unknown. Besides, due to the overlap of the CMASS sample, eBOSS DR14 LRG, and the last data point in BOSS DR12 would have a small correlation of ~ 0.16 (Bautista et al. 2018). Both will lead to a very little influence on the reconstruction results and can hardly alter the constraint on H_0.

[2] We verify that a different assumption of $H_{0,\rm fid}$ hardly varies the inferred $H_{0,\rm rec}$ if we replace $H_{0,\rm fid} = 67.0\,{\rm km\,s^{-1}/Mpc}$ with a different value, such as $H_{0,\rm fid} = 73.0\,{\rm km\,s^{-1}/Mpc}$.

Table 1. Summary of BAO data used.

Data set	$z_{\rm eff}$	Measurements	constraint	unit
6dFGS	0.106	$r_{\rm s}/D_V(z_{\rm eff})$	0.336 ± 0.015	–
BOSS DR12	0.38	$D_{\rm M}(z_{\rm eff})r_{\rm s,fid}/r_{\rm s}$	1512 ± 25	Mpc
		$H(z_{\rm eff})r_{\rm s}/r_{\rm s,fid}$	81.2 ± 2.4	km/s/Mpc
	0.51	$D_{\rm M}(z_{\rm eff})r_{\rm s,fid}/r_{\rm s}$	1975 ± 30	Mpc
		$H(z_{\rm eff})r_{\rm s}/r_{\rm s,fid}$	90.9 ± 2.3	km/s/Mpc
	0.61	$D_{\rm M}(z_{\rm eff})r_{\rm s,fid}/r_{\rm s}$	2307 ± 37	Mpc
		$H(z_{\rm eff})r_{\rm s}/r_{\rm s,fid}$	99.0 ± 2.5	km/s/Mpc
eBOSS DR14 QSO	1.52	$D_V r_{s,fid}/r_{\rm s}$	3843 ± 147	Mpc
eBOSS DR14 LRG	0.72	$D_{\rm A}(z_{\rm eff})r_{\rm s,fid}/r_{\rm s}$	1466.5 ± 136.6	Mpc
		$H(z_{\rm eff})r_{\rm s}/r_{\rm s,fid}$	105.8 ± 16	km/s/Mpc
BOSS DR14 Lyα	2.34	$D_{\rm M}(z_{\rm eff})/r_{\rm s}$	37.41 ± 1.86	–
		$c/(H(z_{\rm eff})r_{\rm s})$	8.86 ± 0.29	–
BOSS DR14 QSOLy α	2.35	$D_{\rm M}(z_{\rm eff})/r_{\rm s}$	36.3 ± 1.8	–
		$c/(H(z_{\rm eff})r_{\rm s})$	9.20 ± 0.36	–

Table 2. Summary of GLTD data. Units of distances are all Mpc.

lens name	z_d	z_s	$D_{\Delta t}$(Mpc)	$D_{\rm A}$(Mpc)	λ	ν	σ
B1608+656	0.6304	1.394	5156^{+296}_{-236}	–	4000	7.053	0.2282
RXJ1131-1231	0.295	0.654	2096^{+98}_{-83}	–	1388.8	6.4682	0.20560
SDSS J1206+4332	0.7545	1.789	5769^{+589}_{-471}	1805^{+555}_{-398}	–	–	–
HE 0435-1223	0.4546	1.693	2707^{+183}_{-168}	–	653.9	7.5793	0.10312

- We use four GLTD distance measurements as summarized in Table 2. The posterior likelihoods of the distance measures for GLTDs B1608+656 (Suyu et al. 2010), RXJ1131-1231 (Suyu et al. 2014), HE 0435-1223 (Wong et al. 2016) and SDSS J1206+4332 (Birrer et al. 2019b) are publicly available. The first three have robust measurements of the time-delay distance, given as skewed log-normal distribution $P(D_{\Delta t}|\boldsymbol{\theta})$:

$$P(D_{\Delta t}|\boldsymbol{\theta}) \approx \frac{1}{\sqrt{2\pi}(\mathrm{x}-\lambda_{\rm D})\sigma_{\rm D}} \times \exp\left[-\frac{(\log(\mathrm{x}-\lambda_{\rm D})-\nu_{\rm D})^2}{2\sigma_{\rm D}^2}\right], \tag{10}$$

where $\boldsymbol{\theta} = \{A_1, B_1, C_1, D_1, \epsilon, r_{\rm s}\}$ for Epsilon model and $\boldsymbol{\theta} = \{A_2, B_2, C_2, D_2, r_{\rm s}\}$ for Log model etc., x is the model prediction of $D_{\Delta t}\,(1\,{\rm Mpc})^{-1}$. $\lambda_{\rm D}$, $\sigma_{\rm D}$ and $\nu_{\rm D}$, which vary for different lenses are summarized in Table 2. For J1206, the time-delay distance and angular diameter distance of the lens $D_{\rm l}$ are both provided, however, as samples of distributions available from the H0LiCOW website[3], for which a kernel density estimator based likelihood is implemented Birrer et al. (2019a) [4].

- We impose a Gaussian prior on $r_{\rm s}$ according to the *Planck* 2015 TT,TE,EE+lowP likelihood combinations (Ade et al. 2016),

$$r_{\rm s} = 147.27 \pm 0.31\,{\rm Mpc}. \tag{11}$$

We do not use the *WMAP9* and the latest *Planck* 18 prior because their $r_{\rm s}$ are consistent with *Planck* 15 and the reconstruction results should not change as also manifested in L18.

3.2. *Inference method*

The best-fitting value of the reconstruction parameters is obtained by minimizing the χ^2 function using the Cosmological MonteCarlo (CosmoMC)[5] (Lewis & Bridle 2002) and analyzed mainly using the GetDist package[6] (Lewis 2019).

[3] https://shsuyu.github.io/H0LiCOW/site/

[4] In the flat ΛCDM model, our best fitting value of H_0 using J1206 alone is 69.94 ± 5.58 - 67.86 ± 6.1 depending on the flat prior of Ω_m and H_0, which is consistent with Birrer et al. (2019a).

[5] https://github.com/cmbant/CosmoMC

[6] https://github.com/cmbant/getdist/releases/tag/1.0.0. We also acknowledge the use of ChainConsumer package (Hinton 2016), available at https://github.com/Samreay/ChainConsumer/tree/Final-Paper.

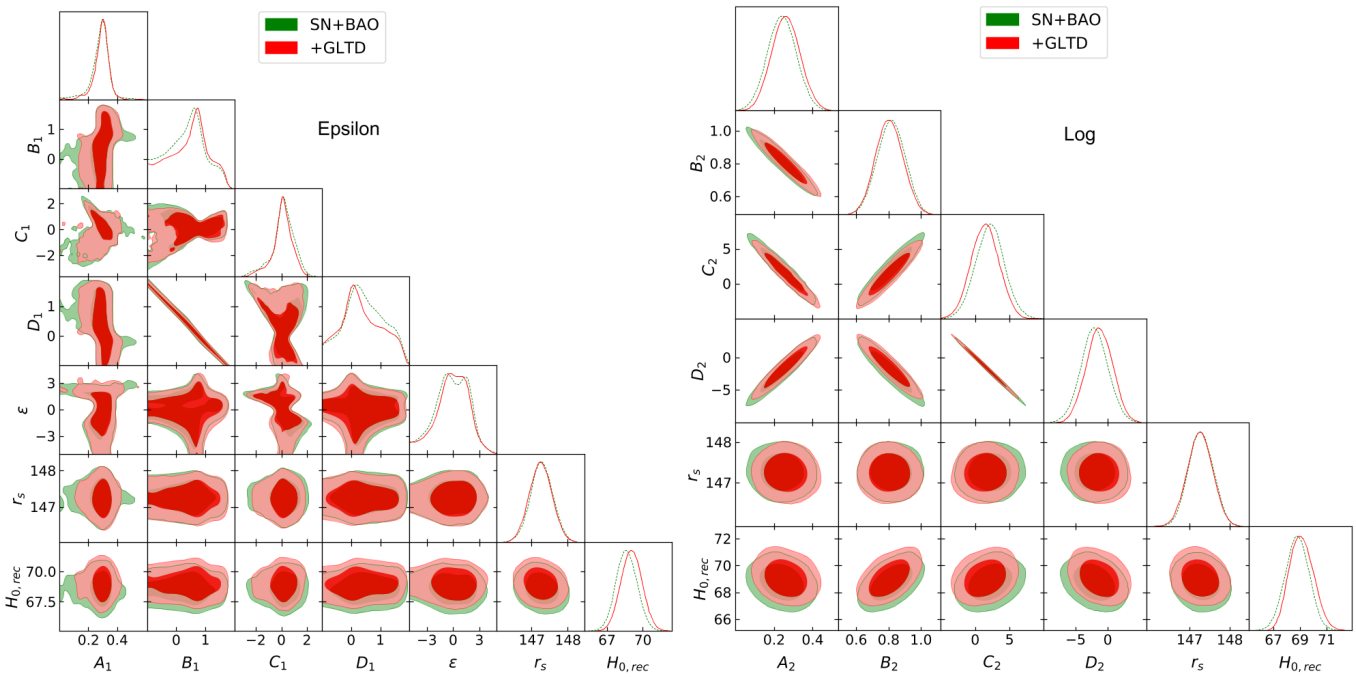

Figure 1. *Left panel*: parameter constraints for the Epsilon model at 68% and 95% C.L. confidence level. *Right panel*: Same as left, but for the Log model. In both the panels we also show $H_{0,\mathrm{rec}}$, which is a derived quantity.

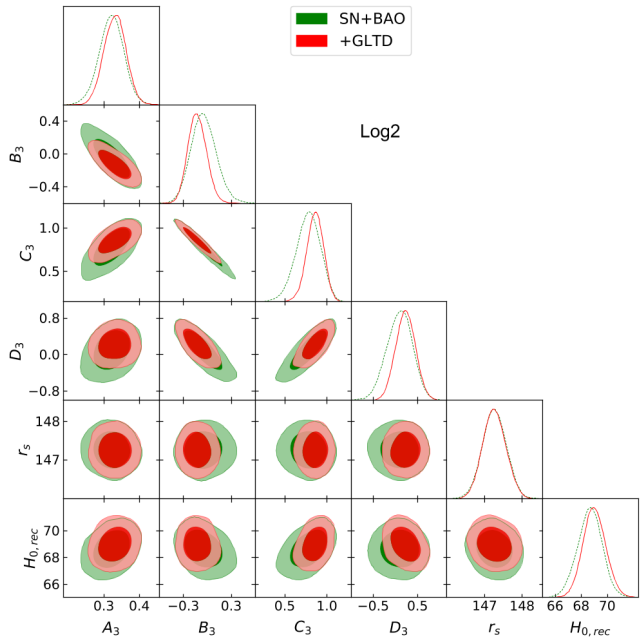

Figure 2. Parameter constraints for the Log2 model at 68% and 95% C.L. limits. Here the parameter B_3 corresponds to curvature. We also show the reconstructed $H_{0,\mathrm{rec}}$.

Given a Gaussian posterior likelihood function (PLF), the general form of χ^2 is

$$\chi^2 = -2\ln(\mathrm{PLF}) = \boldsymbol{\delta}^{\dagger}\mathbf{C}^{-1}\boldsymbol{\delta}, \tag{12}$$

where $\mathbf{C}$ is the covariance matrix of the data, and $\boldsymbol{\delta}$ is the difference between the data and the theoretical predictions. The second expression is valid only when the PLF are Gaussian or approximately Gaussian. In case where PLF is skewed or non-Gaussian, such as the GLTD data mentioned in the Section 3, then we use the first expression. The CosmoMC package has already included the likelihood source file for Pantheon and all BAO measurements except eBOSS DR14 LRG, and we use them directly. For the B1608, J1131, HE0435 GLTD data, we use the PLF described by Equation (10). For the J1206, we first piece-wise divide the chain samples of $D_{\Delta\mathrm{t}}$ and D_d into small bins. Then we calculate the discrete PLF in every 2-dimension bin, the following procedure being the same as for the other data.

We use the Deviance Information Criterion (DIC) to estimate the performance of the four models. DIC combines heritage both from Akaike Information Criterion and Bayesian Information Criterion and applies to parameter degeneracy (Liddle 2007; Spiegelhalter et al. 2002). For a likelihood function $\mathscr{L}$, DIC is defined by

$$\mathrm{DIC} = \overline{\mathrm{D}(\theta)} + \mathrm{p_D} \tag{13}$$

where $\mathrm{D}(\theta) = -2\ln\mathscr{L} + \mathrm{C}$ and $\mathrm{p_D} = \overline{\mathrm{D}(\theta)} - \mathrm{D}(\bar{\theta})$. C is a constant that only depends on data. In this form, definition of DIC has a clear Bayesian interpretation that it deals with average of $\ln\mathscr{L}$ rather than the maximum values. Again, $\mathrm{p_D}$ also has its indication that it approximately equals to the effective number of parameters constrained by the data. If $\mathrm{p_D}$ is less than the number of free parameters of a model ($\mathrm{N_p}$), then it suggests that these parameters are highly degenerate. In Table 4, we also list $\mathrm{p_D}$ for each of the models.

Table 3. Summary of the priors imposed on free parameters for the four models.

model	Epsilon	Log	Log2	$\Omega_{\rm k}\Lambda$CDM
A	$[0.0, 2.0]$	$[0.0, 2.0]$	$[0.1, 0.6]$	$[0.1, 1.0]$
B	$[-2.0, 2.0]$	$[0.0, 2.0]$	$[-0.6, 0.6]$	$[-0.3, 0.3]$
C	$[-5.0, 8.0]$	$[-05.0, 8.0]$	$[0.15, 2.00]$	0
D	$[-2.0, 2.0]$	$[-10.0, 6.0]$	$[-1.0, 5.0]$	$[0.5, 1.2]$
ϵ	$[-5.0, 5.0]$	–	–	–
$r_{\rm s}$	$[130, 160]$	$[130, 160]$	$[130, 160]$	$[130, 160]$

4. Results and Discussion

We assume flat priors on the free parameters, as summarized in Table 3. The constraint results are presented in Table 4 and graphically in Figures 1 to 3 and the mock results are shown in Figure 5.

4.1. *Constraints from current data*

We first use the most recent BAO and Pantheon SN Ia, the constrained results for the Epsilon and Log model are consistent with those reported in L18, with a mild improvement in the accuracy of the parameters due to the newer BAO data. When including the GLTD data, we find no tightening of the constraints, with a mild shift in the marginalized PLF of parameters globally.

The Log model shows highly correlated, however much simpler, Gaussian constraints than the Epsilon model which demonstrates a high degeneracy between the parameters. This degeneracy in the Epsilon model is driven by the parameter ϵ, with a double peak in the marginalized posteriors. In comparison to the results of L18, we notice that the double peak behavior of ϵ is diminished when the prior on B_1, D_1 parameters are extended to negative ranges and completely vanishes when the GLTD data is included, as can be seen in *Left panel* of Figure 1.

The BAO data when combined with the large number of SNIa samples, places tight constraints on the shape of $H(z)$. However, the correlations of the posteriors are compelling, which indicates substantial redundancy of these parameters. To this end, we also estimate the effective number of parameters ($\rm p_D$) constrained, which for the Epsilon model is always less by ~ 1, than the number of free parameters in the likelihood analysis. As shown in Table 4, for the other three models implemented here, the effective number of parameters is almost equivalent to the number of free parameters. This in-turn is one of motivations to utilize the Log model to perform the mock analysis, elaborated later.

Figure 3 describes the evolution of reconstructed $H(z)$, with the $z-$axis in log scale in the limits $z \lesssim 4$. We notice that the Epsilon model in fact extends to negative values of $H(z)$, when extrapolated to larger redshifts. When including GLTD, a rise of $H(z)$ in the low redshift range appears for all models, which results in a slightly higher $H_{0,\rm rec}$ of the order $\Delta H_{0,\rm rec} \sim 0.5$. This is in accordance with the fact that $r_{\rm s}$ prior with the BAO data supersedes the precision with which the GLTD data constrain the present expansion rate.

Both GLTD and BAO+$r_{\rm s}$ can independently determine H_0 while their inference shows mild discrepancy in the flat ΛCDM model (Aghanim et al. 2018; Wong et al. 2019). We plot the constraints from GLTD and BAO+$r_{\rm s}$, as well as their respective combination with SN, i.e., GLTD+SN and BAO+$r_{\rm s}$+SN for the Log model in Figure 4. As expected, the constraints from GLTD on the model parameters are far less stringent. However, it is sufficient to constrain three parameters of interest: A_2, B_2 and $H_{0,\rm rec}$. The constraints from GLTD are consistent with other data sets well within the 1σ region, for the first two parameters. As for the inferred $H_{0,\rm rec}$, we find a mild tension between GLTD and BAO+$r_{\rm s}$. When combined with SN, both, i.e., GLTD+SN and BAO+$r_{\rm s}$+SN data sets prefer lower $H_{0,\rm rec}$ values, while the tension remains since their error bars shrink as well. As shown in Figure 4, when contrasting the constraints form BAO+$r_{\rm s}$ (pink) against SN+GLTD (orange), it is noticeable that the correlation between parameter A_2, which scales as the matter density and $H_{0,\rm rec}$, is negative (i.e, $A_2 \to 0$, for higher values of $H_{0,\rm rec}$) for the former and positive for the latter data set. This in fact results in a lower value of $H_{0,\rm rec}$ in the joint analysis and demonstrates why a low-redshift modification, as in the case of a parametric Log model cannot resolve the H_0-tension. Similar behavior was also earlier noted in Bernal et al. (2016) (see Table 4. therein), using spline based reconstructions, where the SN data along with an $r_{\rm s}$ prior disfavored higher values of H_0, also validating the adequate utility of parametric reconstructions employed here.

Preference for a higher (w.r.t CMB) value of Hubble constant from GLTD is clearly in line with other reports (e.g, Figure 2 and Table 5 in Wong et al. (2019)), also in cases where the Hubble constant is determined via calibrated SN using absolute distances from GLTD (Jee et al. 2019). However, due to its larger uncertainty, at present, it hardly plays a significant role in determining $H_{0,\rm rec}$, in a joint analysis with BAO data. The most recent GLTD data contain 6 gravitationally lensed quasars with updated measurements on both $D_{\Delta \rm t}$ and $D_{\rm d}$ (Wong et al. 2019), for which, the constraints could become even tighter and consequently the tensions could be more even more significant[7].

Next, we consider the models Log2 and $\Omega_{\rm k}\Lambda$CDM (also the reference model), which have a curvature term in their parametric expressions. Figure 2 shows the constraint contours for Log2 model, which are quite similar but with a reduced degeneracy in comparison to the Log model. This is in effect due to the replacement of the linear term with the quadrature term, which now plays the role of curvature. When including the GLTD data, we find a negative curvature parameter B_3, and a larger value for constant parameter C_3, to be compared with the B_2 parameter of the Log model. The effect on the value of $H_{0,\rm rec}$, is similar to that in the Log2 and the Epsilon models. The shape of $H(z)$ for the Log and Log2 model show a major difference at high red-

[7] We were unable to implement the 6 GLTD data set from Wong et al. (2019) here, as they are not yet made publicly available.

Table 4. Summary of the marginalized constraints on the reconstruction parameters and r_s with upper and lower uncertainties at 68% confidence level. We impose flat prior on reconstruction parameters and Gaussian prior on r_s. We also list p_D, which is the effective number of parameters, ΔDIC and $\Delta\chi^2$ w.r.t the $\Omega_k\Lambda$CDM model. All derived quantities are indicated with *. For the reference model we show the DIC and χ^2, for which $\Delta\mathrm{DIC} = \Delta\chi^2 = 0$.

model	Epsilon		Log		Log2		$\Omega_k\Lambda$CDM	
Data set	SN+BAO	+GLTD	SN+BAO	+GLTD	SN+BAO	+GLTD	SN+BAO	+GLTD
A	$0.29^{+0.06}_{-0.05}$	$0.31^{+0.04}_{-0.06}$	$0.24^{+0.07}_{-0.07}$	$0.26^{+0.07}_{-0.07}$	$0.32^{+0.03}_{-0.03}$	$0.33^{+0.03}_{-0.03}$	$0.30^{+0.03}_{-0.03}$	$0.31^{+0.03}_{-0.03}$
B	$0.31^{+0.72}_{-0.87}$	$0.45^{+0.75}_{-0.88}$	$0.81^{+0.09}_{-0.09}$	$0.80^{+0.08}_{-0.08}$	$-0.05^{+0.14}_{-0.17}$	$-0.13^{+0.11}_{-0.12}$	$0.01^{+0.09}_{-0.10}$	$-0.05^{+0.08}_{-0.08}$
C	$0.01^{+1.91}_{-0.61}$	$0.00^{+0.92}_{-0.65}$	$2.11^{+2.07}_{-2.08}$	$1.40^{+2.04}_{-2.03}$	$0.77^{+0.15}_{-0.13}$	$0.86^{+0.11}_{-0.09}$	–	–
D	$0.46^{+0.93}_{-0.79}$	$0.30^{+0.81}_{-0.93}$	$-2.11^{+2.12}_{-2.09}$	$-1.37^{+2.07}_{-2.07}$	$0.09^{+0.30}_{-0.27}$	$0.22^{+0.23}_{-0.21}$	$0.69^{+0.07*}_{-0.06}$	$0.74^{+0.06*}_{-0.06}$
ϵ	$-0.02^{+2.20}_{-1.42}$	$0.11^{+2.09}_{-1.46}$	–	–	–	–	–	–
r_s	$147.26^{+0.31}_{-0.31}$	$147.24^{+0.31}_{-0.31}$	$147.28^{+0.31}_{-0.31}$	$147.23^{+0.31}_{-0.31}$	$147.26^{+0.32}_{-0.32}$	$147.25^{+0.30}_{-0.30}$	$147.25^{+0.31}_{-0.32}$	$147.24^{+0.30}_{-0.30}$
H_0	$68.62^{+0.89*}_{-0.89}$	$69.01^{+0.84*}_{-0.85}$	$68.77^{+0.90*}_{-0.90}$	$69.13^{+0.90*}_{-0.90}$	$68.64^{+0.96*}_{-0.89}$	$69.04^{+0.86*}_{-0.86}$	$68.59^{+0.93}_{-0.95}$	$69.11^{+0.84}_{-0.98}$
p_D	5.16	4.52	4.90	4.88	5.11	4.91	4.02	3.87
ΔDIC(DIC)	+0.82	+1.09	+0.56	+1.91	+2.00	+1.12	1047.80	1053.85
$\Delta\chi^2(\chi^2)$	−1.47	−0.22	−1.21	−0.12	−0.20	−0.97	1039.77	1046.12

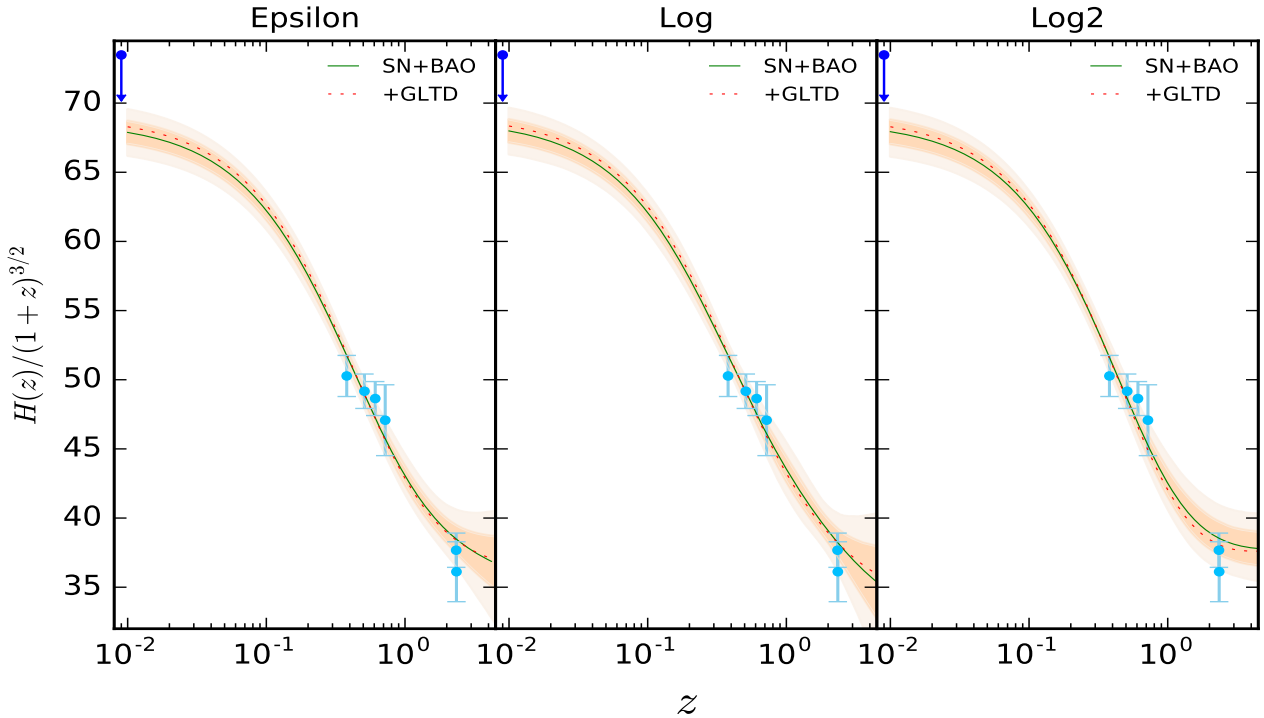

Figure 3. $H(z)$ reconstruction results. The shaded region is the 1σ and 2σ error range of the joint constraint from Pantheon+BAO+GLTD. The light blue points are the BAO estimates of $H(z)$ with its 1σ error. The blue point is the local H_0 measurements and its lower 2σ limit from the distance ladder (Riess et al. 2018).

shifts, where the Log model falls faster with its error bars tending to diverge. While it is not visible when plotting with the −axis in logarithmic, we find that the Log model is, in fact, better driven by the data, which is not the case for the Log2 model whose $H(z)$ evolves more gradually at both extremes of redshift range. This data driven behavior also affirms the aforementioned motivation based on effective number of constrained parameters, to utilize the Log model to perform the mock analyses.

All the numerical results are summarized in Table 4, along with three statistical quantities for the model selection, which are the effective number of model parameters p_D, DIC, and χ^2 at best-fitting value. While p_D is a part of DIC estimate, we list it separately as it estimates the number of parameters of the model that are adequately constrained by the data. For instance, the Epsilon model has the most complicated degeneracy among the parameters of the model. Thus it is expected (and indeed) to have a smaller p_D than the number of

free parameters (i.e, 6). We further find that for every model, p_D always becomes smaller after GLTD is included, which is mostly due to the fact that GLTD is in mild tension with SN and BAO, as shown in Figure 4. Including GLTD would actually increase the freedom, i.e., the degeneracy of free parameters allowed solely by SN or BAO. For the Log model alone we find almost no variation in $p_D(N_p) \sim 4.9(5)$, with the inclusion of the GLTD data set, also being very close to the number of free parameters in the likelihood analysis.

The constraining ability of combined datasets on the four models is similar, having negligible difference in $H_{0,\rm rec}$ estimates. However, we notice that the Log model provides slightly conservative constraints on $H_{0,\rm rec}$, owing to a different behavior with the GLTD dataset. For the Epsilon and Log models, using GLTD alone we find $H_{0,\rm rec} = 80.9 \pm 6.7\,{\rm km\,s^{-1}/Mpc}$ and $H_{0,\rm rec} = 85.1 \pm 7.3\,{\rm km\,s^{-1}/Mpc}$, respectively. Our constraint for the Epsilon model is more similar to the constraint from $w \neq -1$ extension of ΛCDM using the same dataset, recently reported in Taubenberger et al. (2019). The $\Omega_k\Lambda$CDM model is the most optimal fit with the smallest DIC, essentially due to the smallest number of free parameters, having similar χ^2 values to the other models. For instance, with the Log model, $H_{0,\rm rec}$ is obtained by extrapolating the reconstructed $H(z)$ to $z = 0$, for which we find 68% C.L. limits of,

$$H_{0,\rm rec} = 68.77^{+0.90}_{-0.90}\ {\rm km\,s^{-1}/Mpc}\,({\rm SN+BAO}),$$
$$H_{0,\rm rec} = 69.13^{+0.90}_{-0.90}\ {\rm km\,s^{-1}/Mpc}\,({\rm SN+BAO+GLTD}).$$

These values of H_0 in comparison to the *Planck* ΛCDM[8] and local measurement[9] are at $\sim 1.3\sigma$[10] using SN+BAO (1.7σ using SN+BAO+GLTD) and $\sim 2.5\sigma$ (2.3σ), respectively. In the earlier analysis, L18 quote a 1.0σ and 2.7σ for the same comparison with SN+BAO data. However, when the GLTD data are included, our inferences for the respective tensions move in the direction of the results presented in Dutta et al. (2019), whose analyses include Cosmic Chronometers (CC) (Jimenez & Loeb 2002; Moresco 2015) and growth measurements from large scale structure observations.

Although the value of $H_{0,\rm rec}$ is slightly raised by GLTD, they are too small to be consistent with the local measurement of H_0. While this situation would change if the GLTD becomes more accurate and precise, at the current stage, our reconstructed Hubble parameter still favors the *Planck* estimate and is in agreement with other earlier analyses (Aubourg et al. 2015; Bernal et al. 2016; Feeney et al. 2018). Incidentally, we also notice that the H_0 estimates in our analyses, driven by the combination of GLTD data and r_s prior are extremely consistent with those reported in (Haridasu et al. 2018a; Gómez-Valent & Amendola 2018; Mukherjee et al. 2019)[11], which were driven by CC datasets. These earlier results are also model-independent, being very different from the approach implemented here. The low-redshift model-independent (see e.g., Haridasu et al. (2018a)) constraint on the compound parameter $r_s \times H_0/[100\,{\rm km\,s^{-1}/Mpc}]\,({\rm r_s h})$ is consistent with the *Planck* estimate, even with the inclusion of local H_0 (Riess et al. 2018), within 1σ. And also, in line with the earlier analysis performed in Carvalho et al. (2016), we replace the r_s prior with $r_s h = 99.069 \pm 1.598\,{\rm Mpc}$ prior, obtained from the same combination of *Planck* likelihood. This clearly allows for a larger value of $H_0 = 73.86 \pm 2.41\ {\rm km\,s^{-1}/Mpc}$ and a corresponding $r_s = 136.0 \pm 4.5\,{\rm Mpc}$, consistent with Arendse et al. (2019) as expected, and is accompanied by a change in the best-fitting χ^2 value for GLTD data by ~ 3, while the same for SN and BAO data sets remain almost unchanged. In contrast to the $r_s h$ prior, when r_s prior is implemented, as in the main analysis, the posterior estimate of $r_s h = 101.76 \pm 1.32\,{\rm Mpc}$, is driven towards larger values, and consistent with the *Planck* $r_s h$ prior, at $\sim 1.3\sigma$, which is a mild reduction in the H_0 alone $\sim 1.7\sigma$ deviation mentioned earlier.

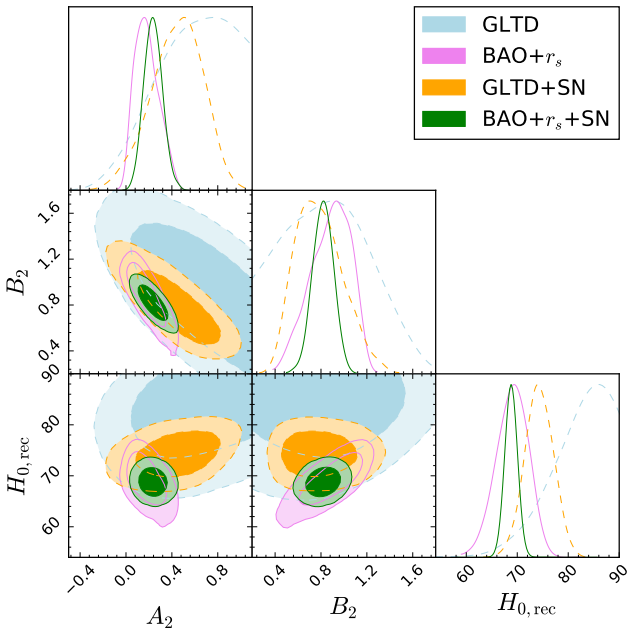

Figure 4. Comparison of constraint results of different data sets for the Log model. All parameters of Log model are free. Here we only report parameters of most interest, A_2, B_2 and $H_{0,rec}$ (see the discussion in the text).

[8] For the same *Planck* likelihood combination utilized for r_s prior here, the corresponding 68 % C.L. limit is $H_0 = 67.27 \pm 0.66\,{\rm km\,s^{-1}/Mpc}$, for the ΛCDM model.

[9] We assume the value of $H_0 = 73.45 \pm 1.66\,{\rm km\,s^{-1}/Mpc}$, from Riess et al. (2018) (hereafter R18).

[10] As is the usual practice in an inverse distance ladder comparison, we assume no correlation between our $H_{0,\rm rec}$ and *Planck* H_0, however, r_s prior is strongly (+0.79) correlated to the latter and our r_s posterior is mildly (−0.14) anti-correlated with the former while being equivalent to the prior. Implying ~ -0.12 anti-correlation between the two H_0 quantities and is expected to increase the deviation and might have a role to play with more precise future data, for instance, increasing to −0.27, in the forecast analysis presented in Section 4.2.

[11] See for example, other works driven by CC based H_0 estimations (Luković et al. 2016; Yu et al. 2017; Luković et al. 2018; Park & Ratra 2019), which at times do not account for the systematics within CC data.

Please note that the r_s prior alone might ensure that the early Universe evolution is fixed to ΛCDM, as any of the one parameter extension such as, $\Omega_k \neq 0$ or $w \neq -1$, would have the same r_s (i.e, same early-time behavior, also validating our use of same prior for the Log2 and Ω_kΛCDM models with curvature freedom), but with a different late-time H_0 (Ade et al. 2016; Verde et al. 2017), consequently a different $r_s h$, w.r.t ΛCDM. This in fact indicates that the early-time behavior constrained from the CMB data while being invariant for such extensions, would imply that the deviations are mainly enhanced when the models are extrapolated to late-time expansion history. However, an $r_s h$ prior from the ΛCDM fit to the CMB data, would necessarily imply a *correlated* early and late time behavior, also allowing for a possibility to break the $r_s - h$ degeneracy differently. As already mentioned, an agreement for the constraint on $r_s h$ from low-redshift BAO and high-redshift CMB, alongside the conformity of higher (than CMB) H_0 values from local distance ladder (R18, Riess et al. (2019)) and GLTD (Wong et al. 2019) data sets[12], taken at a face value (assuming no spurious systematics) would indicate a need for modification of early-time physics. One might tentatively infer that, while an early universe modification as a solution for the H_0-tension is desirable, such a change should necessarily be accompanied with a conserved/invariant $r_s h$ (w.r.t ΛCDM) estimate from CMB, placing an additional restraint on feasible modifications. To this end, the comparison of r_s and $r_s h$ prior analyses helps to assess the extent of allowed variation in the CMB $r_s h$ estimate, from the low-redshift BAO data (also aided by SN). A modification that requires a change in $r_s h$, would also imply a change in angular scales at recombination, which are very well constrained by CMB and subsequently effect the BAO observables, through the assumed fiducial cosmology. In this context, the BAO + Big Bang Nucleosynthesis (BBN) H_0 estimate has been shown to be consistent with the CMB estimate (Aubourg et al. 2015; Addison et al. 2017; Blomqvist et al. 2019; Schöneberg et al. 2019; Cuceu et al. 2019), also in L18, and hints for a modification requiring a change in the $r_s h$ estimate from CMB, which when implemented through the fiducial cosmology in obtaining/rescaling BAO observables, can allow reconciliation with the local H_0 estimate (see also Camarena & Marra (2019)).

4.2. *Constraints from future data*

While the analysis so far, with the up-to-date BAO and GLTD data reaffirms the inferences of L18, we now more importantly forecast the constraining ability of realistic future BAO and GLTD data sets on H_0, through the model-independent formalism. While several future surveys such as Euclid (Amendola et al. 2018) and the Square Kilometre Array (Bacon et al. 2018) can provide precise measurements on BAO (Bengaly et al. 2019; Obuljen et al. 2018), here we focus on BAO from DESI. And GLTD from Large Synoptic Survey Telescope (LSST).

DESI is a Stage IV ground-based experiment started in 2019[13]. It aims at studying BAO and the growth of structure through measuring spectra from 4 target tracers, including luminous red galaxies up to $z \sim 1.0$, bright [O II] emission line galaxies up to $z \sim 1.7$, quasars and Ly-α forest absorption feature in their spectrum up to $z = 3.5$. Following Aghamousa et al. (2016), we use the forecasted BAO measurements, which are quoted as $D_A(z)/r_s$ and $H(z)r_s$, from DESI galaxy, quasar and bright galaxy survey and also assume a correlation coefficient of 0.4 between these two measurements at each redshift.

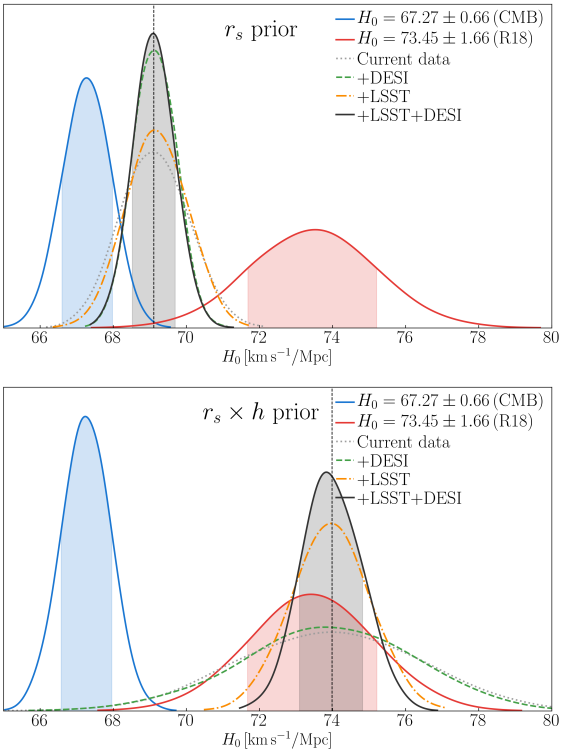

Figure 5. Forecasts of marginalized H_0 using the future data, i.e., BAO from DESI and GLTD data from LSST. The upper panel uses the r_s prior and lower panel implements the $r_s h$ prior, both taken from the same *Planck* likelihood. We choose the fiducial model following the best-fitting of the joint constraint from Pantheon SNIa, BAO and GLTD (i.e., current data). The vertical dashed line represents the mean value from the posterior. It is important to stress the reversal in constraining ability of mock BAO and GLTD data sets, when changing from r_s to $r_s h$ prior.

LSST is an ambitious wide-deep-fast sky survey that plans for regular survey operations by 2022 (Ivezic et al. 2019). Oguri & Marshall (2010) made predictions of the numbers of time-variable sources that should be found by LSST and reported a very positive result that around 3000 of lensed quasars will have well-measured time delays. Based on the catalog of mock lenses in Oguri & Marshall (2010), Jee et al.

[12] Please see Verde et al. (2019) and Riess (2019) for a summary of other low-redshifts probes which imply similar H_0 estimates.

[13] https://www.desi.lbl.gov/

(2016) further forecasted the cosmographic constraints when including both $D_{\Delta t}$ and D_l of lens systems. As the authors anticipated, there should be ~ 55 high-quality quadruple lens systems that have sufficiently good measurements of both distance information. However, this number may vary due to various limitations, for example, telescope observation strategy (Liao 2019). Furthermore, there should be a correlation between the measured $D_{\Delta t}$ and D_l estimates or otherwise one of the distances should have much large uncertainty. Due to the lack of correlation information, in their paper, here we assume that only $D_{\Delta t}$ is available. According to the current four GLTD data, the uncertainty on $D_{\Delta t}$ varies within $\sim 5.8\% - 7.0\%$. Hence, a 5% uncertainty level is achievable as long as we select the lens systems following the same criteria as Jee et al. (2016). The number of forecasted lens systems is conservatively reduced to 40.

We use the distribution of source and lens redshifts from (Jee et al. 2016) and randomly generate 40 lens systems. In principle, the 40 systems produced every time will have mildly different constraining ability depending on the redshift distribution of lenses and sources. We experimentally tested the fluctuation in the expected $\lesssim 1\sigma$ error by repeating MCMC analyses using different sets of mock GLTD data. We find the variation is much smaller than the uncertainty of the inferred H_0[14]. Thus, we use the one-run simulation results as a quantitative estimate of the constraining ability.

The top panel of Figure 5 shows the 1D marginalized posterior of inferred H_0 when combining the current data with the future BAO and GLTD data for the Log model, with the r_s prior, where the relative heights are also indicative of the constraining ability of the data. For convenient comparison, we plot the current constraint in dotted gray. We do not analyze the other three models in detail, as they are not expected to exhibit much difference, which we verify and that the improvement in percentages will remain the same. However, testing the Epsilon model we find that it is less reliable to reproduce the model utilized to create the mock data set, due to stronger intrinsic degeneracy among the parameters.

With the fiducial model being the best-fitting value constrained by BAO data and *Planck* r_s prior, we forecast the performance of upcoming DESI data, where the uncertainty on H_0 shrinks by a factor of ~ 3.7 (from 2.9 to 0.78), i.e., reduces by $\sim 73\%$, which is quite encouraging. The improvement in the uncertainty of H_0 when the current data (SN+BAO+GLTD) are combined with LSST GLTD, DESI BAO, and LSST GLTD+DESI BAO are $\sim 10.8\%$, 37.8%, and 38.3%, respectively, reaching $\sigma_{H_0} \approx 0.56$ uncertainty level. Our estimate of the improved $\sigma_{H_0} \approx 0.80$ with the inclusion of forecasted GLTD data alone, is in agreement with the analysis in Jee et al. (2016)[15]. Tentatively, the improved precision obtained with the future data (DESI+LSST) around the current best-fit model, would imply similar disagreements at the level of $\sim 2.2\sigma$ higher and $\sim 2.5\sigma$ lower value, than the *Planck* ΛCDM and R18 H_0 derived values, respectively. This could imply a possibility for low-redshift ($0.1 \leq z \leq 2.5$) H_0 estimate that is in between the local ($z \leq 0.15$) and high-redshift CMB estimate. As also shown in top panel of Figure 5, the DESI BAO data contribute most to reducing the uncertainty. The LSST GLDT data are important as well, but they are overwhelmed by the BAO data constraining power when combined. Please note that we have not considered the additional distance information of D_l from the GLTD. According to Jee et al. (2016), including the D_l distance would improve the constraint significantly. Earlier forecast shows about 400 systems of robust measured time delay should be discovered by LSST (Liao et al. 2015). We anticipate the future GLTD data will have a much better performance. Please note that the the fiducial cosmology to create the mock data sets being the best-fit of Log model to the current data, we do not study the contest between the GLTD and BAO data sets, but only forecast the precision of the joint constraint from the future low-redshift data.

Finally, we repeat the exercise of replacing the r_s prior with the $r_s h$ prior, as shown in the bottom panel of Figure 5. The most significant improvements of constraints appear when including the mock BAO data using the r_s prior, while the LSST GLTD data provide only mild improvement. In contrast, when using the $r_s h$ prior we find that the DESI BAO mock data, essentially do not provide any improvement to the constraints and that the major effect is driven by LSST GLTD data. This is simply representative of the fact that BAO data does not provide a constraint on H_0 unless r_s is known, either as an assumed prior or by inclusion of a dataset through which it is constrained. Needless to say, the well-constrained higher value of $H_0 = 73.99 \pm 0.80\,\mathrm{km\,s^{-1}/Mpc}$ (Current data+LSST+DESI) is now accompanied by a lower value of $r_s = 135.9 \pm 1.2\,\mathrm{Mpc}$, which is a 0.9% constraint and a major improvement over the 3.3% constraint from the current data.

5. Summary

In the current work, we reconstruct the late-time expansion history of the universe in a cosmological-model-independent way, focusing on the Hubble constant H_0, using the latest SN Ia, BAO, and GLTD data, implementing four different parametric forms. A summary of our results is as follows:

- Assuming the Gaussian prior on r_s from the high-redshift *Planck* estimate for ΛCDM, our deduced value of Hubble constant for the four models are more consistent with the *Planck* ΛCDM, e.g., for the Log model, at $\sim 1.3\sigma$ using SN+BAO (1.7σ using SN+BAO+GLTD) estimate than with the higher-valued local measurement at $\sim 2.5\sigma$ (2.3σ using SN+BAO+GLTD). We find no preference among models having comparable values of DIC and assess the performance of the parametric models.

- With the updated data and also a curvature freedom (Log2 model), we reaffirm the conclusions of L18, that the Hub-

[14] We run 20 separate MCMC analyses and find that the variation in the uncertainty of inferred H_0 relative to the corresponding mean is $\sim 2.5\%$, which should also contain the MCMC sampling noise.

[15] A more recent analysis in Shiralilou et al. (2019), forecasts GLTD performance in an ideal scenario, which we do not compare with here.

ble tension possibly originates from the early universe. However, as the reconstructed $H(z)$, and hence $H_{0,\rm rec}$, is driven by the data (within the available freedom of the parametric models), conclusions remain to be verified with the more stringent future data.

- Inclusion of GLTD data only mildly increases the best-fitting value of $H_{0,\rm rec}$, hardly improving uncertainty, due to the considerably lower constraining power of GLTD data and we assess mild disagreements among low-redshift data combinations. It is expected to yield possibly increased disagreements with the updated GLTD dataset in Wong et al. (2019).

- Replacing the Gaussian $r_{\rm s}$ prior with the $r_{\rm s}h$ prior, we find a significant decrease of $\Delta\chi^2 \sim 3$ of GLTD and a slight reduction for the BAO data. This further aids the argument that the early universe could be responsible for the Hubble tension, especially the comoving horizon $r_{\rm s}$. A comparison of $r_{\rm s}h$ posteriors in these two cases, helps assess the allowed change in the angular scales constrained by CMB.

- More importantly, we anticipate the performance of future BAO and GLTD data from two upcoming experiments, DESI and LSST. When combined with the current data, we infer an improvement in uncertainty of H_0 by $\sim 10.8\%$ and $\sim 37.8\%$, with GLTD and BAO data, respectively. Combining these two future data will provide an improvement in precision by $\sim 38.3\%$, and might incite a need for agreement between local ($z \leq 0.15$), low-redshift ($0.10 \leq z \leq 2.5$) and high-redshift (CMB) H_0 estimates, indicating moderate-level ($\ll 9\%$ of current difference) modifications to both the CMB and local H_0 estimates.

- Replacing the $r_{\rm s}$ prior with the $r_{\rm s}h$ prior in the forecast analysis we find a value of H_0 consistent with R18, and a lower value of $r_{\rm s} = 135.9 \pm 1.2\,{\rm Mpc}$, which is a 0.9% constraint. This is a major improvement from the 3.3% uncertainty, with the current data.

Implementing a multitude of contrasting analyses in a model-independent inverse distance ladder framework, we expect to find a strong degree of complementarity between BAO and GLTD data sets in the near future, which will provide tighter constraints on cosmological models, and also highlight much needed prospects to resolve the H_0-tension and further important evidences to test physically motivated extensions to the ΛCDM model.

Acknowledgments

This work was supported by the National Natural Science Foundation of China under grants Nos. U1931202, 11633001, and 11690023. MV is supported by INFN INDARK PD51 grant and agreement ASI-INAF n.2017-14-H.0. BSH acknowledges financial support by ASI Grant No. 2016-24-H.0.

References

Abbott, T. M. C., et al. 2019, Astrophys. J., 872, L30, 1811.02374
Addison, G. E., Watts, D. J., Bennett, C. L., Halpern, M., Hinshaw, G., & Weiland, J. L. 2017, ArXiv e-prints, 1707.06547
Ade, P. A. R., et al. 2014, Astron. Astrophys., 571, A16, 1303.5076
Ade, P. A. R., et al. 2016, Astron. Astrophys., 594, A13, 1502.01589
Aghamousa, A., et al. 2016, 1611.00036
Aghanim, N., et al. 2018, 1807.06209
Alam, S., et al. 2017, Mon. Not. Roy. Astron. Soc., 470, 2617, 1607.03155
Amendola, L., et al. 2018, Living Rev. Rel., 21, 2, 1606.00180
Archidiacono, M., Hooper, D. C., Murgia, R., Bohr, S., Lesgourgues, J., & Viel, M. 2019, JCAP, 1910, 055, 1907.01496
Arendse, N., Agnello, A., & Wojtak, R. J. 2019, A&A, 632, A91, ADS, 1905.12000
Aubourg, É. et al. 2015, Physical Review D, 92
Bacon, D. J., et al. 2018, Submitted to: Publ. Astron. Soc. Austral., 1811.02743
Ballardini, M., Finelli, F., Umiltà, C., & Paoletti, D. 2016, Journal of Cosmology and Astroparticle Physics, 2016, 067–067
Banihashemi, A., Khosravi, N., & Shirazi, A. H. 2019, Phys. Rev., D99, 083509, 1810.11007
Bautista, J. E. et al. 2018, ApJ, 863, 110, ADS, 1712.08064
Bengaly, C. A. P., Clarkson, C., & Maartens, R. 2019, 1908.04619
Bernal, J. L., Verde, L., & Riess, A. G. 2016, JCAP, 2016, 019
Betoule, M., et al. 2014, Astron. Astrophys., 568, A22, 1401.4064
Beutler, F. et al. 2011, mnras, 416, 3017, ADS, 1106.3366
Birrer, S. et al. 2019a, Monthly Notices of the Royal Astronomical Society, 484, 4726–4753
Birrer, S., et al. 2019b, Mon. Not. Roy. Astron. Soc., 484, 4726, 1809.01274
Blomqvist, M., et al. 2019, Astron. Astrophys., 629, A86, 1904.03430
Camarena, D., & Marra, V. 2019, arXiv e-prints, arXiv:1910.14125, ADS, 1910.14125
Camera, S., Martinelli, M., & Bertacca, D. 2019, Phys. Dark Univ., 23, 100247, 1704.06277
Carvalho, G. C., Bernui, A., Benetti, M., Carvalho, J. C., & Alcaniz, J. S. 2016, Phys. Rev., D93, 023530, 1507.08972
Choi, G., Suzuki, M., & Yanagida, T. T. 2019, 1910.00459
Clarkson, C., Cortês, M., & Bassett, B. 2007, Journal of Cosmology and Astroparticle Physics, 2007, 011–011
Cuceu, A., Farr, J., Lemos, P., & Font-Ribera, A. 2019, Journal of Cosmology and Astroparticle Physics, 2019, 044–044
de Sainte Agathe, V., et al. 2019, Astron. Astrophys., 629, A85, 1904.03400
Di Valentino, E., Bœhm, C., Hivon, E., & Bouchet, F. m. c. R. 2018a, Phys. Rev. D, 97, 043513
Di Valentino, E., Linder, E. V., & Melchiorri, A. 2018b, Phys. Rev., D97, 043528, 1710.02153
Di Valentino, E., Melchiorri, A., Linder, E. V., & Silk, J. 2017a, Phys. Rev., D96, 023523, 1704.00762
Di Valentino, E., Melchiorri, A., & Mena, O. 2017b, Phys. Rev., D96, 043503, 1704.08342
Dutta, K., Roy, A., Ruchika, Sen, A. A., & Sheikh-Jabbari, M. M. 2019, PhRvD, 100, 103501, ADS, 1908.07267
Feeney, S. M., Mortlock, D. J., & Dalmasso, N. 2018, MNRAS, 476, 3861, ADS, 1707.00007
Gómez-Valent, A., & Amendola, L. 2018, JCAP, 2018, 051, ADS, 1802.01505
Haridasu, B. S., Luković, V. V., Moresco, M., & Vittorio, N. 2018a, JCAP, 1810, 015, 1805.03595
Haridasu, B. S., Luković, V. V., & Vittorio, N. 2018b, JCAP, 5, 033, 1711.03929
Hinton, S. R. 2016, The Journal of Open Source Software, 1, 00045, ADS

Hoscheit, B. L., & Barger, A. J. 2017, in American Astronomical Society Meeting Abstracts, Vol. 230, American Astronomical Society Meeting Abstracts #230, 314.05, ADS
Huang, Q.-G., & Wang, K. 2016, Eur. Phys. J., C76, 506, 1606.05965
Icaza-Lizaola, M., et al. 2019, 1909.07742
Ivezic, e., et al. 2019, Astrophys. J., 873, 111, 0805.2366
Jee, I., Komatsu, E., Suyu, S., & Huterer, D. 2016, Journal of Cosmology and Astroparticle Physics, 2016, 031–031
Jee, I., Komatsu, E., & Suyu, S. H. 2015, JCAP, 1511, 033, 1410.7770
Jee, I., Suyu, S., Komatsu, E., Fassnacht, C. D., Hilbert, S., & Koopmans, L. V. E. 2019, 1909.06712
Jimenez, R., & Loeb, A. 2002, ApJ, 573, 37, ADS, astro-ph/0106145
Karwal, T., & Kamionkowski, M. 2016, Phys. Rev., D94, 103523, 1608.01309
Keenan, R. C., Barger, A. J., & Cowie, L. L. 2013, ApJ, 775, 62, ADS, 1304.2884
Kenworthy, W. D., Scolnic, D., & Riess, A. 2019, The Astrophysical Journal, 875, 145
Khosravi, N., Baghram, S., Afshordi, N., & Altamirano, N. 2019, Phys. Rev., D99, 103526, 1710.09366
Ko, P., & Tang, Y. 2016, Phys. Lett., B762, 462, 1608.01083
Kumar, S., & Nunes, R. C. 2016, Phys. Rev. D, 94, 123511
Lemos, P., Lee, E., Efstathiou, G., & Gratton, S. 2019, Mon. Not. Roy. Astron. Soc., 483, 4803, 1806.06781
Levi, M., et al. 2013, 1308.0847
Lewis, A. 2019, arXiv e-prints, arXiv:1910.13970, ADS, 1910.13970
Lewis, A., & Bridle, S. 2002, Physical Review D, 66
Liao, K. 2019, Astrophys. J., 883, 3, 1908.02892
Liao, K. et al. 2015, The Astrophysical Journal, 800, 11
Liddle, A. R. 2007, Mon. Not. Roy. Astron. Soc., 377, L74, astro-ph/0701113
Luković, , V. V., Haridasu, B. S., & Vittorio, N. 2019, MNRAS, 2671, ADS, 1907.11219
Luković, V. V., D'Agostino, R., & Vittorio, N. 2016, A&A, 595, A109, 1607.05677
Luković, V. V., Haridasu, B. S., & Vittorio, N. 2018, Foundations of Physics, 48, 1446, ADS, 1801.05765
Marra, V., Amendola, L., Sawicki, I., & Valkenburg, W. 2013, Phys. Rev. Lett., 110, 241305
Moresco, M. 2015, MNRAS, 450, L16, 1503.01116
Mortsell, E., & Dhawan, S. 2018, JCAP, 1809, 025, 1801.07260
Mukherjee, A., Paul, N., & Jassal, H. K. 2019, JCAP, 2019, 005, ADS, 1809.08849
Narayan, R. 1991, ApJL, 378, L5, ADS
Obuljen, A., Castorina, E., Villaescusa-Navarro, F., & Viel, M. 2018, Journal of Cosmology and Astroparticle Physics, 2018, 004–004
Oguri, M., & Marshall, P. J. 2010, Monthly Notices of the Royal Astronomical Society, no–no
Pan, S., Yang, W., Di Valentino, E., Saridakis, E. N., & Chakraborty, S. 2019, Phys. Rev. D, 100, 103520
Paraficz, D., & Hjorth, J. 2009, arXiv preprint arXiv:0910.5823
Park, C.-G., & Ratra, B. 2019, Ap&SS, 364, 82, ADS, 1803.05522
Poulin, V., Boddy, K. K., Bird, S., & Kamionkowski, M. 2018, Phys. Rev., D97, 123504, 1803.02474
Poulin, V., Smith, T. L., Karwal, T., & Kamionkowski, M. 2019, Phys. Rev. Lett., 122, 221301, 1811.04083
Raveri, M., & Hu, W. 2019, Phys. Rev., D99, 043506, 1806.04649
Raveri, M., Hu, W., Hoffman, T., & Wang, L.-T. 2017, Phys. Rev. D, 96, 103501
Riess, A. G. 2019, Nature Reviews Physics, 2, 10, ADS, 2001.03624
Riess, A. G. et al. 2018, The Astrophysical Journal, 855, 136
Riess, A. G., Casertano, S., Yuan, W., Macri, L. M., & Scolnic, D. 2019, Astrophys. J., 876, 85, 1903.07603
Riess, A. G., et al. 2016, Astrophys. J., 826, 56, 1604.01424
Rossi, M., Ballardini, M., Braglia, M., Finelli, F., Paoletti, D., Starobinsky, A. A., & Umiltà, C. 2019, Physical Review D, 100
Schöneberg, N., Lesgourgues, J., & Hooper, D. C. 2019, JCAP, 2019, 029, ADS, 1907.11594
Scolnic, D. M., et al. 2018, Astrophys. J., 859, 101, 1710.00845
Shanks, T., Hogarth, L. M., & Metcalfe, N. 2019, MNRAS, 484, L64, ADS, 1810.02595
Shiralilou, B., Martinelli, M., Papadomanolakis, G., Peirone, S., Renzi, F., & Silvestri, A. 2019, arXiv e-prints, arXiv:1910.03566, ADS, 1910.03566
Spiegelhalter, D. J., Best, N. G., Carlin, B. P., & Van Der Linde, A. 2002, Journal of the royal statistical society: Series b (statistical methodology), 64, 583
Suyu, S. H., Marshall, P. J., Auger, M. W., Hilbert, S., Blandford, R. D., Koopmans, L. V. E., Fassnacht, C. D., & Treu, T. 2010, ApJ, 711, 201, ADS, 0910.2773
Suyu, S. H., et al. 2014, Astrophys. J., 788, L35, 1306.4732
Taubenberger, S. et al. 2019, A&A, 628, L7, ADS, 1905.12496
Treu, T., & Marshall, P. J. 2016, The Astronomy and Astrophysics Review, 24, 11
Umiltà, C., Ballardini, M., Finelli, F., & Paoletti, D. 2015, Journal of Cosmology and Astroparticle Physics, 2015, 017–017
Vagnozzi, S. 2019, arXiv e-prints, arXiv:1907.07569, ADS, 1907.07569
Verde, L., Bellini, E., Pigozzo, C., Heavens, A. F., & Jimenez, R. 2017, Journal of Cosmology and Astro-Particle Physics, 2017, 023, ADS, 1611.00376
Verde, L., Bernal, J. L., Heavens, A. F., & Jimenez, R. 2017, Mon. Not. Roy. Astron. Soc., 467, 731, 1607.05297
Verde, L., Treu, T., & Riess, A. G. 2019, in Nature Astronomy 2019, 1907.10625
Whitbourn, J. R., & Shanks, T. 2014, MNRAS, 437, 2146, ADS, 1307.4405
Wong, K. C. et al. 2016, Monthly Notices of the Royal Astronomical Society, 465, 4895–4913
Wong, K. C. et al. 2019, arXiv e-prints, arXiv:1907.04869, ADS, 1907.04869
Xia, J.-Q., Li, H., & Zhang, X. 2013, Phys. Rev. D, 88, 063501
Xia, J.-Q., & Viel, M. 2009, JCAP, 2009, 002, ADS, 0901.0605
Yang, W., Pan, S., Di Valentino, E., Nunes, R. C., Vagnozzi, S., & Mota, D. F. 2018, JCAP, 1809, 019, 1805.08252
Ye, G., & Piao, Y.-S. 2020, arXiv e-prints, arXiv:2001.02451, ADS, 2001.02451
Yu, H., Ratra, B., & Wang, F.-Y. 2017, ArXiv e-prints, 1711.03437
Yuan, W., Riess, A. G., Macri, L. M., Casertano, S., & Scolnic, D. 2019, 1908.00993
Zarrouk, P., et al. 2018, Mon. Not. Roy. Astron. Soc., 477, 1639, 1801.03062
Zhao, M.-M., He, D.-Z., Zhang, J.-F., & Zhang, X. 2017, Phys. Rev., D96, 043520, 1703.08456